Stopping and radial flow in central ^{58}Ni+^{58}Ni collisions between 1*A* and 2*A* GeV

B. Hong,[4,*] N. Herrmann,[4,6] J. L. Ritman,[4] D. Best,[4] A. Gobbi,[4] K. D. Hildenbrand,[4] M. Kirejczyk,[4,10] Y. Leifels,[4] C. Pinkenburg,[4] W. Reisdorf,[4] D. Schüll,[4] U. Sodan,[4] G. S. Wang,[4] T. Wienold,[4] J. P. Alard,[3] V. Amouroux,[3] N. Bastid,[3] I. Belyaev,[7] G. Berek,[2] J. Biegansky,[5] A. Buta,[1] J. P. Coffin,[9] P. Crochet,[9] B. de Schauenburg,[9] R. Dona,[9] P. Dupieux,[3] M. Eskef,[6] P. Fintz,[9] Z. Fodor,[2] L. Fraysse,[3] A. Genoux-Lubain,[3] G. Goebels,[6] G. Guillaume,[9] E. Häfele,[6] F. Jundt,[9] J. Kecskemeti,[2] M. Korolija,[6] R. Kotte,[5] C. Kuhn,[9] A. Lebedev,[7] I. Legrand,[1] C. Maazouzi,[9] V. Manko,[8] J. Mösner,[5] S. Mohren,[6] W. Neubert,[5] D. Pelte,[6] M. Petrovici,[1] P. Pras,[3] F. Rami,[9] C. Roy,[9] Z. Seres,[2] B. Sikora,[10] V. Simion,[1] K. Siwek-Wilczyńska,[10] A. Somov,[7] L. Tizniti,[9] M. Trzaska,[6] M. A. Vasiliev,[8] P. Wagner,[9] D. Wohlfarth,[5] and A. Zhilin[7]

(FOPI Collaboration)

[1]*Institute for Nuclear Physics and Engineering, Bucharest, Romania*
[2]*Central Research Institute for Physics, Budapest, Hungary*
[3]*Laboratoire de Physique Corpusculaire, IN2P3/CNRS, and Université Blaise Pascal, Clermont-Ferrand, France*
[4]*Gesellschaft für Schwerionenforschung, Darmstadt, Germany*
[5]*Forschungszentrum Rossendorf, Dresden, Germany*
[6]*Physikalisches Institut der Universität Heidelberg, Heidelberg, Germany*
[7]*Institute for Theoretical and Experimental Physics, Moscow, Russia*
[8]*Kurchatov Institute, Moscow, Russia*
[9]*Institut de Recherches Subatomiques, IN2P3-CNRS/ULP, Strasbourg, France*
[10]*Institute of Experimental Physics, Warsaw University, Poland*

(Received 7 July 1997)

The production of charged pions, protons, and deuterons has been studied in central collisions of ^{58}Ni on ^{58}Ni at incident beam energies of 1.06*A*, 1.45*A*, and 1.93*A* GeV. The dependence of transverse-momentum and rapidity spectra on the beam energy and on the centrality of the collison is presented. It is shown that the scaling of the mean rapidity shift of protons established for between 10*A* and 200*A* GeV at the Brookhaven AGS and the CERN SPS accelerators energies is valid down to 1*A* GeV. The degree of nuclear stopping is discussed; quantum molecular dynamics calculations reproduce the measured proton rapidity spectra for the most central events reasonably well, but do not show any sensitivity between the soft and the hard equation of state. A radial flow analysis, using the midrapidity transverse-momentum spectra, delivers freeze-out temperatures T and radial flow velocities β_r which increase with beam energy up to 2*A* GeV; in comparison to the existing data of Au on Au over a large range of energies, only β_r shows a system size dependence. [S0556-2813(98)04201-0]

PACS number(s): 25.75.Ld

I. INTRODUCTION

One of the main topics of the current relativistic heavy-ion experiments is the determination of the properties of nuclear matter at high densities and temperatures [1–3]. Many interesting effects can happen already at densities just twice normal nuclear matter density that can be reached in collisions at incident energies around 1*A* GeV: The masses of the constituents can be affected by the surrounding medium due to chiral symmetry restoration [3–6], a sizable fraction of the constituents can be excited into hadronic resonances whose lifetime and mutual interactions might be different in comparison to the properties of the free particles, and for a short time the system might form an equilibrated state that could give access to the bulk properties of nuclear matter, i.e., to the fundamental nuclear matter equation of state (EoS) [5,7–9].

Despite many efforts the various effects could not be disentangled so far, although some fascinating observations have been made recently that await a consistent and coherent explanation, e.g., large collective flow [10,11], low entropy production [12], reduced pion multiplicities in heavy systems with respect to small systems [13], and enhanced subthreshold kaon production in central collisions [14]. In order to achieve an understanding of the underlying physics those observations that were obtained at various beam energies and with different systems need to be correlated with each other. This can be done (a) by studying different observables in one system under the same conditions, (b) by comparing the same observable for a variety of incident energies and system sizes. The latter point is particularly interesting since some observables became available from experiments at the much higher beam energies of the Brookhaven AGS and the CERN SPS, where changes in the development of certain observables could be caused by a possible phase transition to the QCD deconfinement state [15]. Hence a consistent comparison over more than two orders of magnitude in beam energy becomes possible.

A prerequisite for the understanding of the high density

*Present address: Korea University, Seoul, South Korea.

and temperature phase of nuclear matter that might have prevailed in the initial stage of the reaction is the knowledge and the description of the final state that reflects the properties when the constituents cease to interact (freeze-out). The freeze-out conditions visible in the distributions of hadrons are very important since they allow one to test concepts like equilibrium and stopping, and therefore are very useful as a constraint for all more elaborated theories.

This paper presents a rather complete set of data for the phase space distribution (transverse momentum p_t and rapidity y) of protons and deuterons as well as pions for the central collisions of ^{58}Ni on ^{58}Ni at incident beam energies between 1A and 2A GeV, a system for which pion [16], kaon [17], and Δ resonance [18] production as well as proton-proton correlations [19] have already been studied. In the following the centrality and beam energy dependence of the momentum space distributions of the most abundant hadrons are discussed in detail. They provide the basic requirements which models need to fulfill, before the discussion of the initial temperature or baryon density can start. Transport model calculations with the IQMD code [20] are compared to the experimental proton and deuteron rapidity distributions. This allows us to address the question of nuclear stopping power, although in a model-dependent way. We present the mean rapidity shift of protons and study whether the known scaling behavior established above 10A GeV [21] is satisfied at lower beam energies. Finally, we interpret the midrapidity data in terms of a thermal model including collective radial flow. In order to facilitate comparison with other data we use the simple assumption proposed by Siemens and Rasmussen [22], although a lot of effort is devoted to the development and application of more realistic expansion scenarios [10,23,24].

II. EXPERIMENT

The experiment was performed at the heavy-ion synchrotron SIS at GSI by bombarding ^{58}Ni beams of 1.06, 1.45, and 1.93A GeV on a fixed ^{58}Ni target of 225 mg/cm^2 (about 1% interaction length), placed in the target position of the FOPI detector, which is described in detail elsewhere [25,26]. For the analysis presented in this paper we used the central drift chamber (CDC) of FOPI for particle identification, and its forward plastic wall for the centrality determination. This azimuthally symmetric forward wall covers the polar angles θ_L from 7° to 30°, measuring the deposited energy and the time of flight and hence the charge of the fragments. The multiplicity of these fragments, called PMUL in the following, was used for the selection of the event centrality. The CDC covers the θ_L angles from 30° to 150°. Pions, protons, and deuterons were identified in the chamber by means of their mean energy loss $\langle dE/dx\rangle$ and their laboratory momentum p_L, obtained from the curvature of the particle tracks in the field of a 0.6 T magnet. The accuracy of the position measurements of the tracks in radial and azimuthal direction via drift time was $\sigma_{r\phi}\simeq 400$ μm. The position resolution along the beam direction by charge division was less accurate ($\sigma_z\simeq 4$ cm for protons and deuterons and 10 cm for pions). The resolution of the mean energy loss, $\sigma(\langle dE/dx\rangle)/\langle dE/dx\rangle$, was about 15% for minimum ionizing particles. The resolution of the transverse momentum p_t, $\sigma(p_t)/p_t$, was about 4% for $p_t<0.5$ GeV and worsened to 12% near $p_t\simeq 2$ GeV. The phase space covered by the chamber is shown in Fig. 1 for the identified $\pi^{\pm}$, protons, and deuterons at 1.93A GeV. Throughout the paper we use the normalized transverse momentum $p_t^{(0)}\equiv p_t/(\gamma_{\rm cm}\beta_{\rm cm}m_0)$ and the normalized rapidity $y^{(0)}\equiv y/y_{\rm cm}-1$. Here $y_{\rm cm}$ and $\beta_{\rm cm}$ are the rapidity and velocity of the center of mass (c.m.), $\gamma_{\rm cm}=1/\sqrt{1-\beta_{\rm cm}^2}$, and m_0 is the rest mass of the considered particles (we use the convention $\hbar=c=1$).

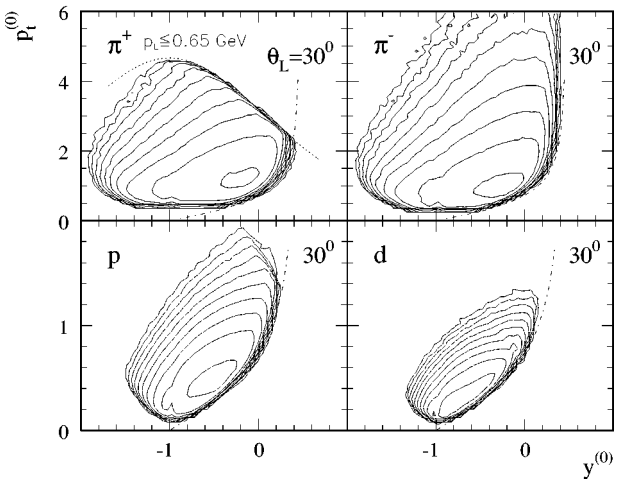

FIG. 1. Acceptance of $\pi^{\pm}$, protons and deuterons at 1.93A GeV under a centrality cut of 420 mb on PMUL (see text). With the definition of $y^{(0)}$, -1, $+1$ and 0 denote the target, projectile, and the c.m. rapidity. Each successive contour line represents a relative factor of two in terms of yields. The dash-dotted lines show the geometrical limit of the drift chamber at $\theta_L=30°$, while the dotted line for π^+ shows the high $p_{\rm Lab}$ cut imposed by the separation against the protons.

III. PARTICLE SPECTRA

For a more quantitative investigation we present, in Fig. 2 π^-, proton and deuteron spectra in $\Delta y^{(0)}$ bins of width 0.1. Chosen were two bins at target and at midrapidity for the reaction at 1.93A GeV, selected by a cut on the upper end of the PMUL distribution representing the most central 100 mb of cross section (the selectivity of such PMUL cuts on the impact parameter is discussed later). The data are plotted in a Boltzmann representation, i.e., $1/m_t^2\cdot d^2N/dm_t dy^{(0)}$ vs m_t-m_0, in which a thermalized system is expected to show a single-exponential shape in the absence of flow; $m_t=\sqrt{p_t^2+m_0^2}$ is the transverse mass of the considered particle. As shown by the dashed lines, the π^- spectra can be well described by the sum of two exponential functions, while the proton and deuteron spectra are compatible with one exponential function in our acceptance (with deviations in the range of very low p_t in the target-rapidity bin):

$$\frac{1}{m_t^2}\frac{d^2N}{dm_t dy^{(0)}} = \begin{cases} C_l\cdot e^{-m_t/T_{Bl}}+C_h\cdot e^{-m_t/T_{Bh}} & \text{for } \pi^- \\ C\cdot e^{-m_t/T_B} & \text{for } p \text{ and } d. \end{cases} \quad (1)$$

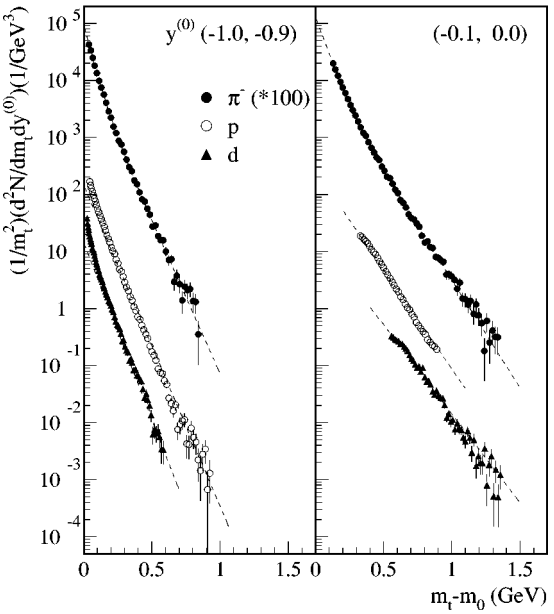

FIG. 2. Boltzmann spectra (absolute yield per event) of π^- (solid circles), protons (open circles), and deuterons (solid triangles) at target rapidity ($y^{(0)}$ from -1.0 to -0.9, left) and at midrapidity ($y^{(0)}$ from -0.1 to 0.0, right). The data are for 1.93*A* GeV collisions with a cut of 100 mb on PMUL. The π^- specta are multiplied by 100 for a clearer display. The dashed lines show the fits with the sum of two exponentials for pions and with one exponential for protons and deuterons.

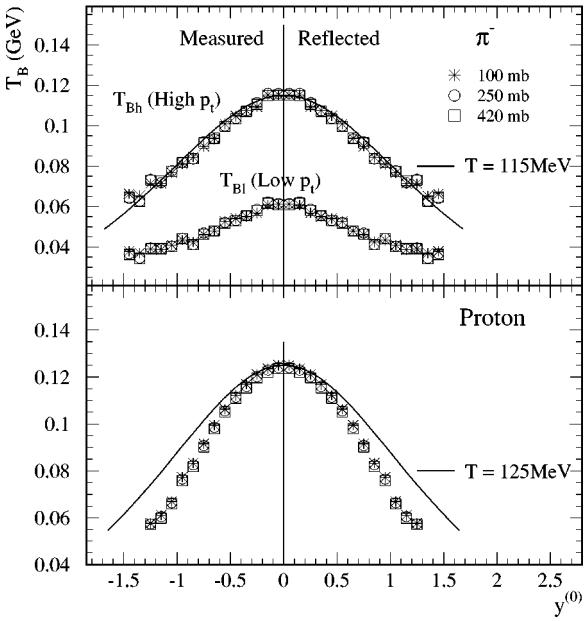

FIG. 3. Centrality dependence of the Boltzmann slope parameter T_B for π^- (separately for the low- and high-p_t component) and protons at 1.93*A* GeV. The solid lines are the results of the isotropic expansion model without collective radial flow. For details see Sec. V.

Here, C is a normalization constant, T_B is the Boltzmann slope parameter, and the subscripts l and h denote the fitting parameters of the π^--spectra in the low- and high-p_t range, respectively. The enhancement of pions at low p_t can be understood in terms of the $\Delta(1232)$ resonance decay and in fact can be used to determine the number of $\Delta(1232)$ at freeze-out [18,27]. The enhancement above the single-exponential fit near zero p_t at target rapidity in the proton and deuteron spectra, which was already observed at the BEVALAC [28], and at much higher energies at the AGS [29], is attributed to spectator contributions. That is why it is seen only at target rapidity; it disappears as soon as the window is moved by a step of only 0.2 in $y^{(0)}$ towards midrapidity. To obtain the rapidity distributions $dN/dy^{(0)}$, we integrated the fitted functions of Eq. (1) from $p_t=0$ to ∞ in order to account for the missing part in the acceptance (cf. Fig. 1). Because of the fact that we did not try to include the mentioned low-m_t enhancement of protons and deuterons near target rapidity (Fig. 2) the resultant rapidity distributions are expected to represent primarily the distribution of *participant* matter to which our prime interest is addressed.

In the spectra presented in this paper only the statistical errors are shown. The systematic errors in the $dN/dy^{(0)}$ distributions are different for each particle species and vary with the beam energy and rapidity, the largest values existing for the midrapidity data at 1.93*A* GeV, mainly due to the smallest geometrical acceptance. At this energy the integration over the complete p_t range leads to estimated errors of about 2, 5, and 20% for pions, protons, and deuterons at midrapidity, respectively. These values were determined by using three different possibilities, i.e., an exponential shape in Boltzmann and invariant representations and the thermal model including the radial flow [Eq. (4) in Sec. V]. The uncertainty in the tracking efficiency (10%) was obtained by visual inspection of several hundred event displays and by comparing the results of an analysis with different tracking algorithms [13]. The uncertainty in the particle identification (2%) was determined by changing the software criteria. Assuming that the sources of these different errors add incoherently, we obtain maximal systematic errors for the $dN/dy^{(0)}$ distributions of 10, 11, and 23% for pions, protons, and deuterons, respectively. A confirmation that the extrapolation procedure over the full p_t range is reasonable is the integrated charge of all reaction products up to ^{4}He which for the most central collisions (100 mb) agrees within 10% with the total charge of the system no matter which spectral form is assumed. The systematic error in T_B, caused by the different tracking methods and the different fitting range in p_t is estimated to about 5%.

A. Centrality dependence

The centrality dependence was studied in the case of the reaction at 1.93*A* GeV. Figures 3 and 4 show the T_B and $dN/dy^{(0)}$ distributions for different cuts on PMUL thereby varying the selected cross section between the most central 100 and 420 mb, representing 4 and 15% of the total reaction cross section, respectively. The relation between the centrality cuts and the impact parameter b as calculated within the IQMD model are summarized in Table I. Note that the data are measured only for $y^{(0)}<0$, and then reflected about midrapidity, using the symmetry of the colliding system. It is apparent that the T_B distributions of Fig. 3 are practically identical for the three centrality cuts both for protons and for each of the two-pion components, whereas in Fig. 4 a relatively modest enhancement of the midrapidity yield is ob-

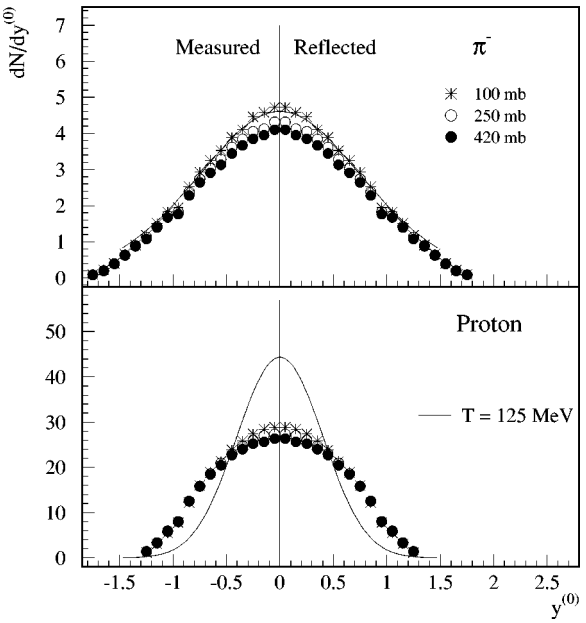

FIG. 4. Centrality dependence of the $dN/dy^{(0)}$ spectra for π^- and protons at 1.93*A* GeV. The solid lines are the results of the isotropic expansion model without collective radial flow. For details see Sec. V.

served with increasing centrality in the $dN/dy^{(0)}$ distributions of both particles, somewhat more pronounced in case of the pions. When cutting even sharper on centrality we find a saturation of the pion value at about 30 mb, while the proton distribution remains stable below 100 mb. The lack of dramatic changes below an effective sharp-cut impact parameter of about 4 fm indicates a limited impact parameter resolution when using the PMUL selection in a relatively small system such as Ni+Ni.

In the case of global thermal equilibrium one expects the following characteristic rapidity dependence of the slope parameter T_B

$$T_B(y) = T/\cosh(y) \tag{2}$$

leading to a bell-shaped curve for T_B with $T_B = T$ at midrapidity ($y = 0$). This dependence, adjusted to the experimental T_B (125 MeV for protons) at midrapidity, is compared to the experimental results in the lower panel of Fig. 3. It is evident that the data are not described by this global equilibrium assumption; this scenario, *which neglects flow*, would rather imply that baryonic matter is ''colder'' away from midrapidity. The failure of the purely thermal scenario is also evident from the experimental proton $dN/dy^{(0)}$ distributions (lower panel Fig. 4): they are much wider than the calculated one for an isotropically emitting thermal source of 125 MeV temperature.

In contrast to the protons we find that the T_B and $dN/dy^{(0)}$ distributions of the high m_t component of the pions *are* compatible with an apparent global temperature which is however somewhat lower ($T_\pi = 115$ MeV) than implied by the midrapidity value of T_B for the protons (see Figs. 3 and 4). When including the deuteron data (Figs. 5 and 6) into the considerations one notices at midrapidity a pronounced increase of T_B with the mass of the particle.

The fact that the *full* rapidity distributions of protons indicate incomplete thermalization, while the pion rapidity distributions appear to be ''thermal'' could indicate any or a combination of both of the following possibilities: only a (midrapidity) fraction of the nucleons are part of a thermally equilibrated fireball that comprises most of the pions *or* alternatively, there is no fully equilibrated fireball, as suggested by the nucleonic distributions, while the $dN/dy^{(0)}$ distributions of the rather light pions are insensitive to this nonthermal behavior. Exploring the first possibility, but not definitely excluding the second we shall see later that it is possible to describe the *midrapidity* m_t spectra of protons, deuterons, and pions with a common temperature if one introduces *flow* (see Sec. V). *As we shall see, isotropic flow does not, however, remedy the problem of understanding the width of the baryonic rapidity distribution.*

B. Beam energy dependence

Figures 5 and 6 show the beam energy dependence of T_B and $dN/dy^{(0)}$ distributions of π^-, protons, and deuterons under a PMUL cut of 100 mb. Generally one finds larger T_B values, especially near midrapidity, when going from 1.06 to 1.93*A* GeV. The high-p_t slope parameter T_{Bh} of the π^- spectra changes more than the low-p_t slope parameter T_{Bl} (an increase at midrapidity of 24% compared to only 11%). The increase becomes larger for the heavier particles (30% for protons and 34% for deuterons), which hints to a larger flow velocity at the higher beam energies. Remarkably there is no significant change of T_B with beam energy near target (projectile) rapidity. In case of the rapidity distributions $dN/dy^{(0)}$ of Fig. 6, we find that the spectra of protons and deuterons exhibit similar shapes at the different energies. This implies that the width of the baryon $dN/dy^{(0)}$ spectra is rather independent of the beam energy, which will be addressed further in the next section. The inverse slope param-

TABLE I. Centrality cuts on the PMUL distributions, related cross sections σ, and the corresponding impact parameters b, calculated with the IQMD model with hard equation of state (EoS) and a momentum-dependent potential. The nuclear radius $R(A)$ is given by $1.2A^{1/3}$, where A is the number of nucleons; the maximum impact parameter $b_{\max}$ is determined by $\sqrt{\sigma/\pi}$.

System	$R(A)$(fm)	PMUL	σ(mb)	$b_{\max}$(fm)	$\langle b \rangle_{\mathrm{IQMD}}$(fm)
		$\geqslant 25$	420	3.7	2.6
1.93*A* GeV Ni+Ni	4.7	$\geqslant 31$	250	2.8	2.1
		$\geqslant 37$	100	1.8	1.6
1.06*A* GeV Au+Au	7.0	$\geqslant 76$	120	2.0	2.8

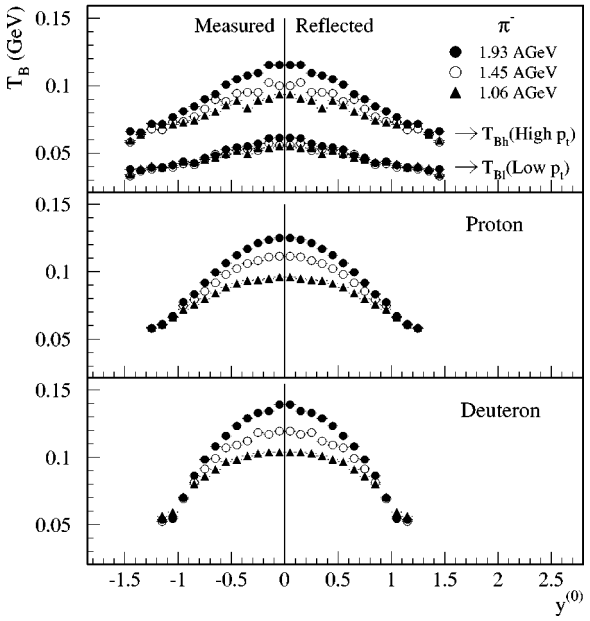

FIG. 5. Beam energy dependence of the Boltzmann slope parameter T_B for π^- (low- and high-p_t component), protons, and deuterons under a cut of 100 mb on PMUL.

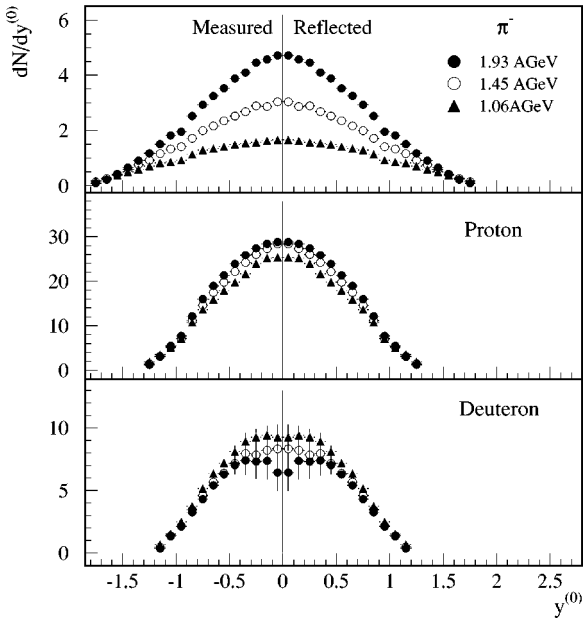

FIG. 6. Beam energy dependence of the $dN/dy^{(0)}$ spectra for π^-, protons, and deuterons with a cut of 100 mb on PMUL. For the deuteron data the error bars denote the systematic errors due to the different extrapolations towards $p_t=0$.

eters at midrapidity and the integrated particle yields per event are summarized in Table II. For a more thorough discussion of the pion yields and the systematic errors affecting them we refer to [13,16].

IV. BARYON RAPIDITY SPECTRA

Baryon rapidity distributions allow a view on the stopping power of nuclear matter, provided the uncertainties introduced by the limited knowledge of the collision geometry can be controlled. Especially for the present light system, finite particle number fluctuations are important when trying to select head-on collisions. In order to understand the properties of our selection criterion PMUL, we first compare the proton and deuteron $dN/dy^{(0)}$ spectra with the IQMD model [20].

A. Comparison with IQMD

As an example we compare in Fig. 7 the experimental $dN/dy^{(0)}$ distributions of protons and deuterons at 1.93*A* GeV for the most central PMUL cut (100 mb) to IQMD model results, obtained with the option of a hard EoS (compression constant $K=380$ MeV) and a momentum-dependent potential, IQMD(HM). The solid lines represent the model results under the same centrality cut as the data, i.e., a PMUL cut on the upper 100 mb in the charged-particle multiplicity spectra for $7°\leqslant\theta_L\leqslant30°$. *Using instead an impact parameter cut corresponding geometrically to the 100 mb multiplicity cut, i.e., $b<1.8$ fm, does not affect the theoretical predictions. Within the model, it is possible to estimate the impact parameter resolution achieved in the experiment: this is shown by a contour plot of the predicted impact parameter vs multiplicity (PMUL) correlation (Fig. 8). A resolution of about 2 fm can be inferred. On the other hand, IQMD predicts that the rapidity distributions do not change for impact parameter cuts below 2 fm. Presumably, this is due to large fluctuations in this relatively small system.* We conclude that the uncertainty imposed by using PMUL as a centrality criterion instead of the exact *b* is very small for protons as well as deuterons.

Composite particles from the model were formed by a space coordinate cluster algorithm after an elapsed collision time of 200 fm/*c* using the standard distance parameter of 3 fm. Under these conditions IQMD underpredicts the deuteron-to-proton ratio by approximately a factor of 5.

TABLE II. Inverse slope parameters at midrapidity T_B^0 and integrated particle yields per event with a cut on PMUL of 100 mb (cf. Table I). For pions the two slopes with index *l* and *h* refer to the low- and high-p_t part of the spectra. Only the dominant systematic errors are quoted. The statistical errors are about 20 and 10% of the systematic errors of T_B^0 and the yields, respectively.

	π^-		Proton		Deuteron	
E_{beam}/A(GeV)	T_{Bl}^0/T_{Bh}^0 (MeV)	Yield	T_B^0 (MeV)	Yield	T_B^0 (MeV)	Yield
1.06	55±3/93±5	3.6±0.4	96±5	38.4±4.2	104±5	14.4±2.4
1.45	56±3/100±5	5.8±0.6	111±6	41.6±4.6	120±6	12.8±2.6
1.93	61±3/115±6	8.5±0.9	125±6	44.0±4.8	139±7	11.6±2.4

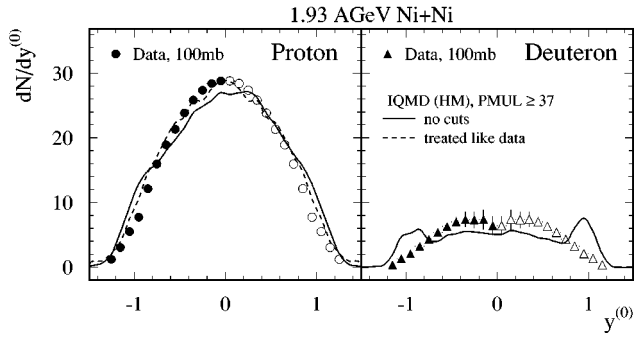

FIG. 7. Comparison of experimental proton (left) and deuteron (right) $dN/dy^{(0)}$ spectra (symbols) with results of the IQMD(HM) model at 1.93*A* GeV (solid and dashed lines). The solid IQMD curves were obtained under the same cut on PMUL as in the data analysis disregarding all acceptance cuts, the dashed line for the protons was obtained applying the same procedure as used for the data.

Since we wish to emphasize the shapes of the rapidity distributions all model calculations are normalized to the integral of the data in the figure. The small ''spectator'' shoulder for protons in the model (or the slight peak in the case of the deuterons) is not seen in the data because, as mentioned earlier, the spectator components of the proton and deuteron spectra at low p_t are suppressed by our integration. *This explanation was confirmed in the case of protons by applying the same fit and integration procedure (dropping the low-p_t spectator component) to the IQMD events. The result, shown by the dashed line in the left panel of Fig. 7, is in excellent agreement with the data. For the deuteron spectrum the low statistics of the IQMD calculations did not allow us to apply the same procedure as for the data.* The comparison of measured and simulated $dN/dy^{(0)}$ spectra of protons and deuterons in the case of the other beam energies shows a similar degree of agreement for the 100 mb cut. Therefore, we conclude that the IQMD model reproduces the shape of the measured proton $dN/dy^{(0)}$ spectra at the most central collisions. IQMD calculations with a soft EoS ($K=200$ MeV) and momentum-dependent potential, IQMD(SM), show very similar results as the IQMD(HM) version, so there is no sensitivity to the stiffness of the EoS in the proton and deuteron rapidity spectra.

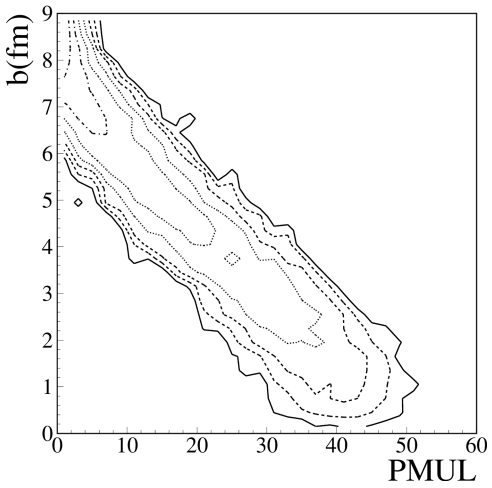

FIG. 8. Contour plot of the impact parameter versus multiplicity (PMUL) correlation. The contour levels are increasing by a factor of 2.5 with each line from the outside to the inside of the distribution.

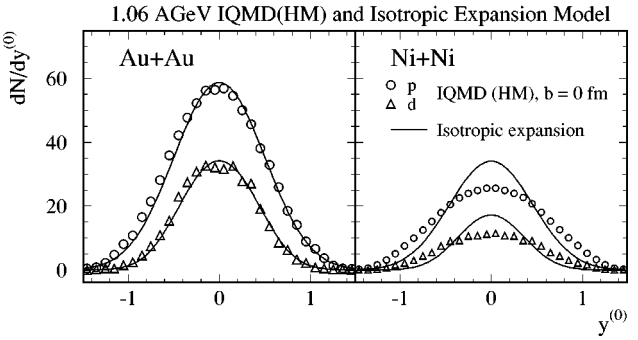

FIG. 9. Comparison of $dN/dy^{(0)}$ spectra from the IQMD(HM) model (symbols) with results of the isotropic expansion model (solid lines) for the systems Au+Au (left) and Ni+Ni (right), both at 1.06 A GeV. The IQMD results are for zero impact parameter ($b \leq 0.5$ fm for Au+Au, $b=0$ for Ni+Ni). The isotropic expansion model uses the parameters given in Table III for Ni+Ni and those of Ref. [11] for Au+Au.

Based on these observations, we compare in Fig. 9 the $dN/dy^{(0)}$ model predictions for protons and deuterons in Ni+Ni collisions (right panel) calculated for zero impact parameter in the IQMD model with results of the isotropic expansion model, using the parameters given in Sec. V (Table IV). Also shown are IQMD predictions for Au+Au collisions of the same energy of 1.06*A* GeV (left panel) together with the result of an isotropic expansion scenario using the parameters $T=81$ MeV and $\beta_r=0.32$ at 1.0*A* GeV from Ref. [11]. In the IQMD model the widths of the $dN/dy^{(0)}$ distributions of protons and deuterons in Au+Au are narrower than in Ni+Ni collisions at the same beam energy. Additionally, the $dN/dy^{(0)}$ for Au+Au collisions can be described nicely by the isotropic expansion model, while the one for Ni+Ni is wider than the model, in accordance with our experimental findings (cf. Fig. 4).

In principle, one cannot distinguish incomplete stopping from a longitudinal expansion after full stopping on the basis of the rapidity spectra alone. However, the systematic comparison of the $dN/dy^{(0)}$ spectra between the small and large colliding system within the IQMD model, the results of which are supported by our experimental data in the case of the most central Ni+Ni collisions, can help to resolve this ambiguity. The narrower $dN/dy^{(0)}$ shape of Au+Au as compared to Ni+Ni for $b=0$ fm indeed tells us that the IQMD model predicts a partial transparency for the latter system. One would expect a wider $dN/dy^{(0)}$ distribution or a smaller mean rapidity shift δy_p (as defined in the next section) for heavier colliding systems in case of a longitudinal expansion after full stopping. Using the same model, this subject was investigated by Bass *et al.* by means of the $(n-p)/(n+p)$ ratio in the isospin-asymmetric system ^{50}Cr+^{48}Ca, where a partial transparency was also predicted at an energy of 1*A* GeV [30].

B. Scaling of the mean rapidity shift of protons

Recently, Videbæk and Hansen discussed the systematics of the baryon rapidity losses in central nucleus-nucleus col-

TABLE III. Summary of the mean rapidity shift of protons (see text for definition). Note that the present analysis includes protons and deuterons. The numbers in parenthesis are the results from the IQMD model calculations with a hard EoS.

$E_{\rm beam}/A$(GeV)	y_b	System	$\sigma/\sigma_{\rm tot}$(%)	δy_p	$\delta y_p/y_b$	Reference
1.06	1.388	Ni+Ni	3.6	0.389	0.280	This work
			($b=0$ fm)	(0.394)	(0.284)	IQMD(HM)
1.06	1.388	Au+Au	($b\leqslant 0.5$ fm)	(0.432)	(0.311)	IQMD(HM)
1.45	1.586	Ni+Ni	3.6	0.453	0.285	This work
1.93	1.782	Ni+Ni	3.6	0.503	0.282	This work
			($b=0$ fm)	(0.521)	(0.292)	IQMD(HM)
11.6	3.21	Au+Au	4.0	1.02	0.32	Ref. [21]
14.6	3.44	Si+Al	7.0	0.97	0.28	Ref. [21]
200	6.06	S+S	3.0	1.69	0.28	Ref. [21]

lisions at AGS and SPS energies [21]. The main conclusion was that the mean rapidity losses scaled with the beam rapidity from 10*A* to 200*A* GeV. In this section we want to study whether this scaling behavior holds at the present lower beam energies, too, i.e., down to 1*A* GeV.

Table III summarizes the results of our analysis and the one of Ref. [21] in terms of the mean rapidity shift of protons (δy_p) defined as

$$\delta y_p \equiv \frac{\int_{-\infty(y_{\rm cm})}^{y_{\rm cm}(\infty)} |y - y_{t(b)}| (dN_p/dy) dy}{\int_{-\infty(y_{\rm cm})}^{y_{\rm cm}(\infty)} (dN_p/dy) dy}, \tag{3}$$

where y_t and y_b represent the target and beam rapidities, respectively, and dN_p/dy is the proton rapidity distribution. The quantity δy_p reflects the inverse width of the rapidity distribution: The more protons, or baryons in general, pile up at the c.m. rapidity, the higher are the δy_p values. The scaled shift $\delta y_p/y_b$ is shown in Fig. 10 as a function of beam energy. For the relatively smaller systems (Ni+Ni at the SIS, Si+Al at the AGS, and S+S at the SPS) $\delta y_p/y_b$ is constant for the beam energies between 1*A* and 200*A* GeV, which implies that the shape of the baryon $dN/dy^{(0)}$ spectra is independent of the beam energies over this energy range. For the heavier system (Au+Au) both the IQMD prediction at 1*A* GeV and the data at 11*A* GeV show a slightly larger $\delta y_p/y_b$, which means a higher concentration of baryons at midrapidity.

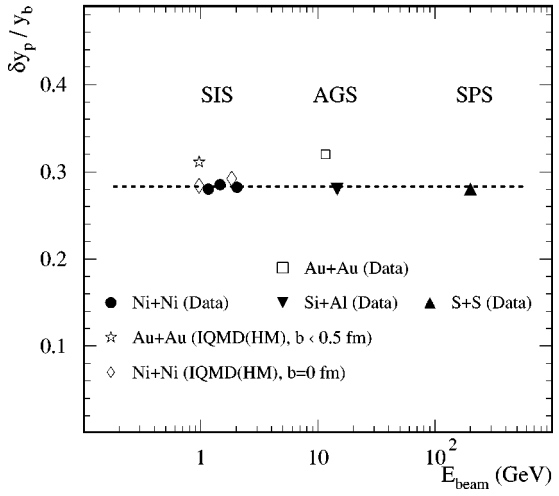

FIG. 10. Mean rapidity shift of protons scaled with the beam rapidity as a function of beam energy. The dashed straight line at 0.28 is only to guide the eye. The data of the AGS and SPS experiments are from Ref. [21].

V. RADIAL FLOW

There has been a lot of effort to understand the collective motion in heavy-ion collisions, hoping to get a handle on the nuclear equation of state [2]. Especially the radial flow of the midrapidity fireball as an important energy carrier [10,11,24,31–33] has been studied extensively. In this section we want to extract the temperature T and the average radial flow velocity β_r from the midrapidity transverse-momentum spectra. We employ the formula of the simple thermal blast model proposed by Siemens and Rasmussen [22]:

$$\frac{1}{m_t^2}\frac{d^2N}{dm_t dy^{(0)}} \propto \cosh y \; e^{-\gamma_r E/T} \times \left[\left(\gamma_r + \frac{T}{E}\right)\frac{\sinh\alpha}{\alpha} - \frac{T}{E}\cosh\alpha\right], \tag{4}$$

with $\gamma_r = 1/\sqrt{1-\beta_r^2}$ and $\alpha = (\gamma_r \beta_r p)/T$, where $E = m_t \cosh y$ and $p = \sqrt{p_t^2 + m_t^2 \sinh^2 y}$ are the total energy and momentum of the particles in the c.m. system. In this model, the thermally equilibrated system expands isotropically, then freezes out suddenly at which time all the particles in the system share a common local T and β_r.

We are aware that the full event topology is *not* isotropic and the ansatz Eq. (4) can therefore at best describe a part of the populated phase space which we restrict to the midrapidity interval ($-0.1 < y^{(0)} < 0.0$) under the 100 mb PMUL cut. This should minimize the contaminations by spectators and nonisotropic flow components (Fig. 4). The effect of the collective flow can be more significant for heavier particles as seen at lower beam energy [10,33], but at the present energies composite particles are so few that we restrict the analysis to pions, protons, and deuterons. For such light particles it was shown in Ref. [10] that details of the flow profile are not discernible because the thermal fluctuations wash them out. This justifies the use of the Siemens-Rasmussen formula

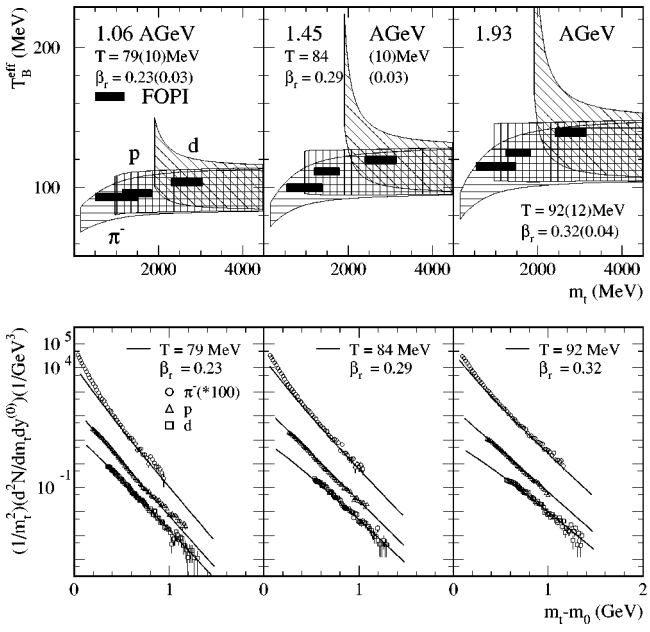

FIG. 11. Top: $T_B^{\rm eff}$ vs m_t of calculations (see text for details) within the isotropic expansion model spanned by the given parameters of T and β_r for π^- (horizontally hatched), proton (vertically hatched), and deuteron (diagonally hatched) at three beam energies. Bottom: Measured Boltzmann spectra compared to the model calculations (solid lines). Note that the π^- spectrum is multiplied by 100 for a clearer display.

which replaces the integration over a complex flow velocity profile by a single ''representative'' velocity β_r. On the other hand, the contamination of the proton and deuteron spectra by products evaporated from the heavier fragments is largely reduced in the energy range we are studying here. Besides simplicity, an important benefit of this simple-minded fit to the data is that a direct comparison with the results of a very similar analysis for the Au+Au system [11] can be done.

Applying the definition of a slope parameter in Eq. (1) to Eq. (4), we evaluate an effective slope $T_B^{\rm eff}$ from the model as follows:

$$T_B^{\rm eff} \equiv -\left[\frac{d}{dm_t}\left\{\ln\left(\frac{1}{m_t^2}\frac{d^2N}{dm_t dy^{(0)}}\right)\right\}\right]^{-1}. \qquad (5)$$

Here $T_B^{\rm eff}$ shows a combined effect of T and β_r, and the model gives the estimate of $T_B^{\rm eff}$ at each m_t value. In the top panel of Fig. 11, our data are shown by bold lines (the fitting errors are smaller than the thickness of each line) together with the model calculations. The m_t range of the fit to the experimental data, which is another important constraint in determining the model parameters, is also indicated. We include only T_{Bh} of π^- since the low-p_t component of the pion spectra is strongly affected by the $\Delta(1232)$ decay [18,27]. To determine T and β_r, the two parameters were varied until the model describes our experimental data; the resulting values are summarized in Table IV. The top panel of Fig. 11 displays the range of the model calculations for π^- (horizontally hatched), protons (vertically hatched) and deuterons (diagonally hatched). Having determined T and β_r, we confirm the results by comparing the spectra from the model with the data directly as shown in the bottom panel of Fig. 11. The results were also checked by the simultaneous fitting method requiring a minimum χ^2 per degree of freedom, and they are consistent with each other within 5%.

TABLE IV. Summary of radial flow velocities β_r and freeze-out temperatures T for the high-p_t part of the pion spectra and of the proton and deuteron distributions in Ni+Ni collisions for the studied energies, derived within the model of Siemens and Rasmussen [22]. The parameters T_C and μ_B from the chemical equilibrium model [34] are also included.

$E_{\rm beam}/A$(GeV)	β_r	T (MeV)	T_c (MeV)	μ_B
1.06	0.23 ± 0.03	79 ± 10	73 ± 10	780 ± 30
1.45	0.29 ± 0.03	84 ± 10	81 ± 10	755 ± 25
1.93	0.32 ± 0.04	92 ± 12	90 ± 13	725 ± 35

Before discussing the results in the framework of general flow systematics it is worthwhile to check on two points: (1) Could the fact that resonances other than the $\Delta(1232)$ are excited (but not explicitly treated in the analysis of the high momentum part of the pion spectra) strongly modify the analysis, and (2) In view of the fact that the spectral shape analysis requires only (local) *thermal* equilibrium, can we check that the particle *yields* are consistent with *chemical* equilibrium?

We have studied both questions in the context of a hadrochemical equilibrium model [32,34]. The model parameters, chemical freeze-out temperature T_c and baryon chemical potential μ_B, are treated as free parameters, and fixed to reproduce the experimental yields of nucleons, deuterons, thermal pions, $\Delta(1232)$ [18] and η mesons from $N^\star(1535)$ resonances [35]. The extracted parameters, T_c and μ_B, are also shown in Table IV (for a comparison of the model results with experimental particle yield ratios, see [18]). At all energies the temperature T derived from the spectra including flow agrees with the chemical freeze-out temperature T_c obtained from the particle yields within 8% [34]. The extracted baryon chemical potentials correspond to roughly 0.5 ± 0.2 of the saturation density ($0.17\ {\rm fm}^{-3}$).

The effects due to higher resonances were estimated using fixed average masses. Within this model, the total freeze-out population of $N^\star(1440)$, $N^\star(1520)$, and $N^\star(1535)$ is estimated to be less than 10% of the $\Delta(1232)$ population at 1.93A GeV. For freeze-out densities of approximately half the normal nuclear matter density, the contribution of thermal pions compared to the number of pions from resonances with masses larger than the $\Delta(1232)$ resonance exceeds the latter by more than a factor of 10. Therefore it is reasonable to assume in the analysis that the high-p_t component of pion spectra is due to the thermal pions.

Figure 12 shows the comparison of the model parameters T and β_r and the fraction of the total available energy per nucleon in c.m. contained in the radial flow motion [$E_{r\rm flow}/E_{\rm cm}$, with $E_{r\rm flow}=(\gamma_r-1)m_N$ and m_N being the nucleon mass] from the current analysis with other results for the system Au+Au [10,11,33]. Before drawing conclusions from the data presented in Fig. 12 the reader should be aware of the specific differences in the experimental analyses. While the present analysis used midrapidity pion (high-T component), proton, and deuteron spectra, the EOS collabo-

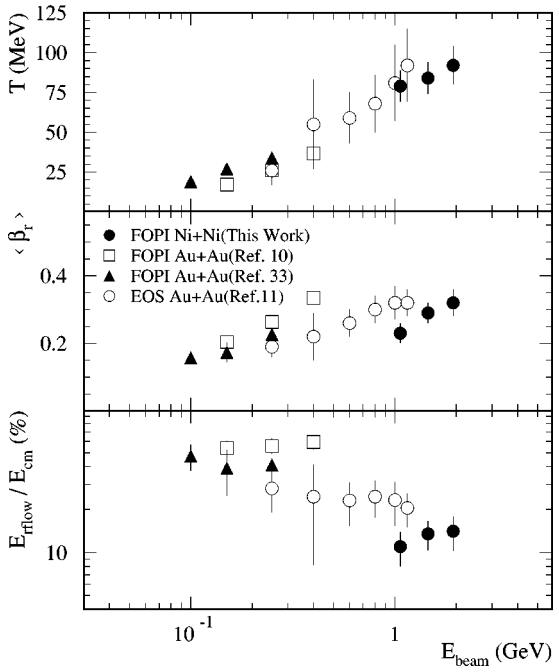

FIG. 12. Compilation of results of various experiments, showing T, β_r and $E_{r\mathrm{flow}}/E_{\mathrm{cm}}$, the fraction of available c.m. energy contained in radial flow, as function of the beam energy.

ration [11] based their conclusions primarily on the 90° (c.m.) spectra of $A=2$, 3, and 4 fragments, but otherwise the same formalism was used as described here. The flow analysis of Ref. [33] was based essentially on a comparison of the mass dependence of the average kinetic energies of $Z=1$ fragments (i.e., p,d,t). The temperatures were derived in a more indirect way with the help of simulations taking into account evaporation; for the values cited in the figure a freeze-out density of 80% of the ground-state density was used which gave the best overall reproduction of the spectral shapes of all the $Z=1$ and 2 isotopes. Concerning the flow velocities of Ref. [33] we have added a Coulomb correction to the published values. The analysis of [10] was extended to fragments with $Z=2-8$ and to the full measured phase space allowing for a more complex flow profile under the additional constraint of energy conservation.

While some of the straggling in the data points shown in Fig. 12 could well be due to the different methods and data types used to extract the parameters, one can nevertheless discern some general trends. First of all we find that both T and β_r increase monotonically as a function of beam energy up to 2A GeV for both colliding systems. Secondly the temperature T seems to be independent of the system, while the radial flow velocity β_r is larger for the larger system size (at least close to 1A GeV). Intuitively this system size dependence of β_r is consistent with our conclusion of the nuclear stopping power in the previous section. The larger nuclei have a larger stopping power, accumulate more pressure in the midrapidity fireball, and as a result the system expands faster. The fact that the freeze-out temperature turns out to be the same for the Ni as for the Au system does not necessarily mean that the primordial temperature, prior to expansion, was the same. As a matter of fact, within the picture of an adiabatic expansion following maximal compression, one is tempted to conclude that the primordial temperature was somewhat higher in the Au system since the larger collective energy at freeze-out in the heavier system indicates a stronger conversion of thermal energy, hence a stronger cooling. If this tentative interpretation is true, then participant matter in the Ni system, even around midrapidity, has not thermalized as thoroughly as in the Au system at the stage of maximal compression. This shows the necessity to study system size dependences in order to assess quantitatively the degree of equilibration in such collisions.

As a third point we wish to emphasize that the flow energy represents a sizable fraction of the available energy E_{cm} (lower panel of Fig. 12). In the context of the present work we note that the flow energy in the Ni system (13% of E_{cm} as mean value of the three Ni points) is about half as large as that deduced for the Au system at a comparable energy. From the yields and temperatures (Tables II and IV), we estimate that the baryons take up 50% (at 1.06A GeV), respectively 35% (at 1.93A GeV) of E_{cm} as thermal energy, pion production consumes about 10% (at 1.06A GeV), respectively 17% (at 1.93A GeV).

While the introduction of radial flow allows us to describe the midrapidity proton spectra with a significantly reduced (local) temperature, as compared to a static thermal scenario, it turns out that this does not affect the predicted baryonic rapidity distributions: hence, as shown before in Fig. 4, the large width of this distribution cannot be accounted for. A simple energy balance consideration then leads to the conclusion that a significant fraction (approximately 30%) of E_{cm} is left in surplus longitudinal movement of the leading baryons for relatively small colliding systems such as Ni+Ni. One should, however, not argue too strongly about the precision of these numbers: the different analysis methods imposing the energy conservation, freeze-out density, and flow velocity profiles may favor different sets of T and β_r.

VI. CONCLUSIONS

We have studied in detail the π^-, proton, and deuteron spectra for central Ni+Ni collisions at beam energies between 1A and 2A GeV. We do not observe any dependence of the slope parameter of the transverse momentum spectra on the event centrality (from 420 to 100 mb), while a higher pion production and a stronger proton concentration at midrapidity is seen for more central events.

The slope parameters are generally larger for higher beam energies, and the effect is more pronounced for the heavier particles; the pion slope parameter for the high transverse-momentum component changes more than the one of the low transverse-momentum component. The rapidity spectra of protons and deuterons show very similar shapes at the different bombarding energies under the same centrality cuts. These shapes are however incompatible with global thermal equilibrium.

The IQMD model can reproduce the measured proton and deuteron rapidity spectra for the most central events, with very similar results for the option of a hard and soft equation of state. The rapidity spectra of protons and deuterons from the IQMD in Au+Au are narrower than in Ni+Ni for vanishing impact parameter, which implies more nuclear stopping power in the larger colliding system. The known scaling

law for the mean rapidity shift of protons (scaled with the beam rapidity) is satisfied down to 1*A* GeV for small colliding systems.

The freeze-out temperature and radial flow velocity of midrapidity particles increase with the beam energy up to 2*A* GeV, but only the radial flow velocity shows a system size dependence. The energy fraction consumed by the radial flow motion is constant for a given colliding system size at beam energies between 0.1*A* and 2*A* GeV. In Ni+Ni collisions this energy fraction is about one half of the value found in Au+Au collisions.

ACKNOWLEDGMENTS

We would like to thank Professor Peter Braun-Munzinger for many discussions and proofreading of the manuscript. This work was supported in part by the Bundesministerium für Forschung und Technologie under Contracts No. 06 HD 525 I(3), 06 DD 666 I(3), X051.25/RUM-005-95, and X081.25/N-119-95.

[1] R. Stock, Phys. Rep. **135**, 259 (1986).
[2] H. Stöcker and W. Greiner, Phys. Rep. **137**, 277 (1986).
[3] G. E. Brown, Phys. Rep. **163**, 167 (1988).
[4] M. Lutz, A. Steiner, and W. Weise, Nucl. Phys. **A574**, 755 (1994).
[5] G. Q. Li and C. M. Ko, Phys. Lett. B **349**, 405 (1995).
[6] J. Aichelin and C. M. Ko, Phys. Rev. Lett. **55**, 2661 (1985).
[7] P. J. Siemens and J. I. Kapusta, Phys. Rev. Lett. **43**, 1486 (1979).
[8] R. Stock, R. Bock, R. Brockman, J. W. Harris, A. Sandoval, H. Stroebele, and K. L. Wolf, Phys. Rev. Lett. **49**, 1236 (1982).
[9] J. W. Harris *et al.*, Phys. Lett. **153B**, 377 (1985); Phys. Rev. Lett. **58**, 463 (1987).
[10] W. Reisdorf *et al.*, FOPI Collaboration, Nucl. Phys. **A612**, 493 (1997).
[11] M. A. Lisa *et al.*, EOS Collaboration, Phys. Rev. Lett. **75**, 2662 (1995).
[12] C. Kuhn *et al.*, FOPI Collaboration, Phys. Rev. C **48**, 1232 (1993).
[13] D. Pelte *et al.*, FOPI Collaboration, Z. Phys. A **357**, 215 (1997).
[14] D. Miskowiec *et al.*, KaoS Collaboration, Phys. Rev. Lett. **72**, 3650 (1994).
[15] For example, see ''Stopping and Flow,'' in Proceedings of Quark Matter '96 Conference, Heidelberg, Germany, 1996 [Nucl. Phys. **A610**, 49 (1996)].
[16] D. Pelte *et al.*, FOPI Collaboration, Z. Phys. A **359**, 55 (1997).
[17] J. Ritman *et al.*, FOPI Collaboration, Z. Phys. A **352**, 355 (1995).
[18] B. Hong *et al.*, FOPI Collaboration, Phys. Lett. B **407**, 115 (1997).
[19] R. Kotte *et al.*, FOPI Collaboration, Z. Phys. A **359**, 1 (1997).
[20] S. A. Bass, C. Hartnack, H. Stöcker, and W. Greiner, Phys. Rev. C **51**, 3343 (1995).
[21] F. Videbæk and O. Hansen, Phys. Rev. C **52**, 2684 (1995).
[22] P. J. Siemens and J. O. Rasmussen, Phys. Rev. Lett. **42**, 880 (1979).
[23] P. Danielewicz, Phys. Rev. C **51**, 716 (1994).
[24] M. Petrovici *et al.*, FOPI Collaboration, Phys. Rev. Lett. **74**, 5001 (1995).
[25] A. Gobbi *et al.*, FOPI Collaboration, Nucl. Instrum. Methods Phys. Res. A **324**, 156 (1993).
[26] J. Ritman for the FOPI Collaboration, Nucl. Phys. B, Proc. Suppl. **44**, 708 (1995).
[27] W. Weinhold, Ph.D. thesis, TH Darmstadt, 1996; W. Weinhold, B. L. Friman, and W. Nörenberg, GSI Scientific Report 96-1 (1996), p. 67.
[28] A. Sandoval *et al.*, Phys. Rev. C **21**, 1321 (1980).
[29] J. Barrette *et al.*, E814 Collaboration, Z. Phys. C **59**, 211 (1993); Phys. Rev. C **50**, 3047 (1994).
[30] S. A. Bass, J. Konopka, M. Bleicher, H. Stöcker, and W. Greiner, GSI Scientific Report 94-1 (1995), p. 66.
[31] S. C. Jeong *et al.*, FOPI Collaboration, Phys. Rev. Lett. **72**, 3468 (1994).
[32] P. Braun-Munzinger, J. Stachel, J. P. Wessels, and N. Xu, Phys. Lett. B **344**, 43 (1995); **356**, 1 (1996).
[33] G. Poggi *et al.*, FOPI Collaboration, Nucl. Phys. **A586**, 755 (1995).
[34] B. Hong, Proceedings of the International Research Workshop on Heavy Ion Physics, Poiana Brasov, Romania, 1996, World Scientific (unpublished).
[35] F.-D. Berg *et al.*, TAPS Collaboration, Phys. Rev. Lett. **72**, 977 (1994); M. Appenheimer *et al.*, GSI Scientific Report 96-1 (1996), p. 47.